



Deposited via The University of Leeds.

White Rose Research Online URL for this paper:

<https://eprints.whiterose.ac.uk/id/eprint/146500/>

Version: Accepted Version

Article:

Pulingam, T, Thong, KL, Ali, ME et al. (2019) Graphene oxide exhibits differential mechanistic action towards Gram-positive and Gram-negative bacteria. *Colloids and Surfaces B: Biointerfaces*, 181. pp. 6-15. ISSN: 0927-7765

<https://doi.org/10.1016/j.colsurfb.2019.05.023>

(c) 2017, Elsevier Ltd. This manuscript version is made available under the CC BY-NC-ND 4.0 license <https://creativecommons.org/licenses/by-nc-nd/4.0/>

Reuse

This article is distributed under the terms of the Creative Commons Attribution-NonCommercial-NoDerivs (CC BY-NC-ND) licence. This licence only allows you to download this work and share it with others as long as you credit the authors, but you can't change the article in any way or use it commercially. More information and the full terms of the licence here: <https://creativecommons.org/licenses/>

Takedown

If you consider content in White Rose Research Online to be in breach of UK law, please notify us by emailing eprints@whiterose.ac.uk including the URL of the record and the reason for the withdrawal request.

Graphene Oxide Exhibits Differential Mechanistic Action towards Gram-positive and Gram-negative Bacteria

Thiruchelvi Pulingam ^a, Kwai Lin Thong ^b, Md. Eaqub Ali ^a, Jimmy Nelson Appaturi ^a

Ignatius Julian Dinshaw ^a, Zhan Yuin Ong ^c, Bey Fen Leo ^{a,d*}

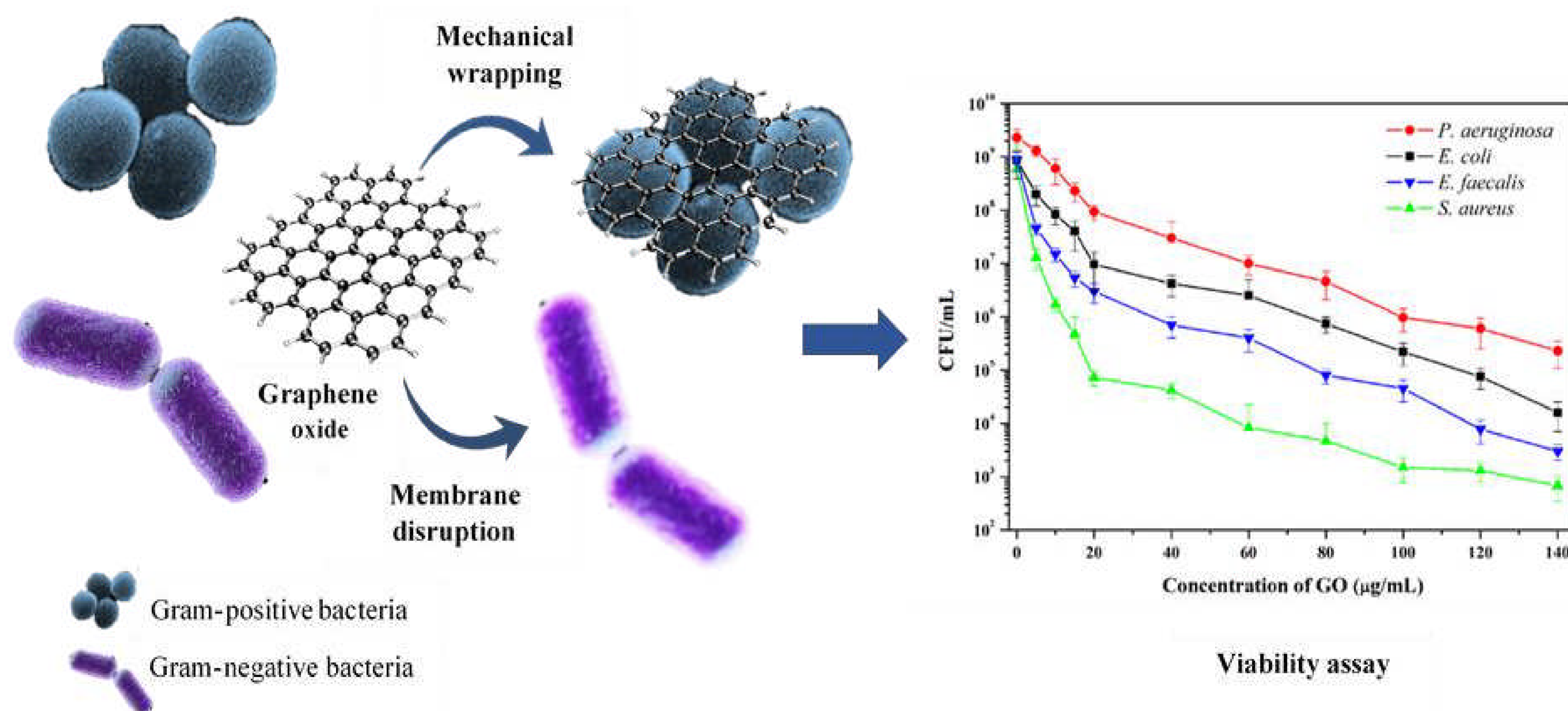
^a *Nanotechnology & Catalysis Research Centre (NANOCAT), Institute of Graduate Studies, University of Malaya, 50603 Kuala Lumpur, Malaysia.*

^b *Institute of Biological Sciences, Faculty of Science, University of Malaya, 50603 Kuala Lumpur, Malaysia.*

^c *School of Physics and Astronomy and Leeds Institute of Biomedical and Clinical Sciences, School of Medicine, University of Leeds, Leeds LS2 9JT, U.K.*

^d *Faculty of Medicine, University of Malaya, 50603 Kuala Lumpur, Malaysia.*

Graphical Abstract



Highlights

- Antibacterial activity of GO towards bacteria are concentration and time-dependent.
- GO shows differential bactericidal activity towards bacteria.
- Mechanical wrapping was noted for *Staphylococcus aureus* and *Enterococcus faecalis*.
- Membrane disruptions was observed for *Escherichia coli* and *Pseudomonas aeruginosa*.

1 **Graphene Oxide Exhibits Differential Mechanistic Action towards Gram-** 2 **positive and Gram-negative Bacteria**

3 Thiruchelvi Pulingam ^a, Kwai Lin Thong ^b, Md. Eaqub Ali ^a, Jimmy Nelson Appaturi ^a

4 Ignatius Julian Dinshaw ^a, Zhan Yuin Ong ^c, Bey Fen Leo ^{a,d*}

5 ^a *Nanotechnology & Catalysis Research Centre (NANOCAT), Institute for Advanced*
6 *Studies, University of Malaya, 50603 Kuala Lumpur, Malaysia.*

7 ^b *Institute of Biological Sciences, Faculty of Science, University of Malaya, 50603*
8 *Kuala Lumpur, Malaysia.*

9 ^c *School of Physics and Astronomy and Leeds Institute of Biomedical and Clinical*
10 *Sciences, School of Medicine, University of Leeds, Leeds LS2 9JT, U.K.*

11 ^d *Faculty of Medicine, University of Malaya, 50603 Kuala Lumpur, Malaysia.*

12

13

14

Abstract

15 The antibacterial nature of graphene oxide (GO) has stimulated wide interest in the medical
16 field. Although the antibacterial activity of GO towards bacteria has been well studied, a
17 deeper understanding of the mechanism of action of GO is still lacking. The objective of the
18 study was to elucidate the difference in the interactions of GO towards Gram-positive and
19 Gram-negative bacteria. The synthesized GO was characterized by Ultraviolet-visible
20 spectroscopy (UV-VIS), Raman and Attenuated Total Reflectance-Fourier-transform infrared
21 spectroscopy (ATR-FTIR). Viability, time-kill and Lactose Dehydrogenase (LDH) release
22 assays were carried out along with FESEM, TEM and ATR-FTIR analysis of GO treated
23 bacterial cells. Characterizations of synthesized GO confirmed the transition of graphene to
24 GO and the antibacterial activity of GO was concentration and time-dependent. Loss of
25 membrane integrity in bacteria was enhanced with increasing GO concentrations and this
26 corresponded to the elevated release of LDH in the reaction medium. Surface morphology of
27 GO treated bacterial culture showed apparent differences in the mechanism of action of GO
28 towards Gram-positive and Gram-negative bacteria where cell entrapment was mainly
29 observed for Gram-positive *Staphylococcus aureus* and *Enterococcus faecalis* whereas
30 membrane disruption due to physical contact was noted for Gram-negative *Escherichia coli*
31 and *Pseudomonas aeruginosa*. ATR-FTIR characterizations of the GO treated bacterial cells
32 showed changes in the fatty acids, amide I and amide II of proteins, peptides and amino acid
33 regions compared to untreated bacterial cells. Therefore, the data generated further enhance
34 our understanding of the antibacterial activity of GO towards bacteria.

35 *Keywords: antibacterial activity, graphene oxide, mechanism of action, mechanical*
36 *wrapping, membrane damage*

37 * Corresponding author.

38 *E-mail address: beyfenleo@um.edu.my (B.F. Leo).*

39

40

41

42

43

44

45

46

47 **1. Introduction**

48 Graphene oxide (GO) is one of the promising materials that has been reported to have
49 excellent antibacterial properties due to its easy and low cost of preparation and ability to be
50 produced in a large-scale [1-3]. GO is the preferred nanomaterial in the biomedical field over
51 other carbon allotropes because of its stability in colloidal form and the reliability of
52 graphene's aqueous dispersibility when it is in a single or multi-layered state [4]. Ever since
53 the first medical application of GO was demonstrated in the field of drug delivery in 2008,
54 the research initiative in exploring other uses of graphene material in the biomedical field has
55 been increasing exponentially [5-7].

56 The prevalence of multidrug-resistant pathogens has reduced the availability of
57 effective drugs for the treatment of serious bacterial infections. Hence there has been intense
58 interest to look for antimicrobial agents with alternative mechanisms of action. Metal/metal
59 oxide nanomaterial such as silver, gold, titanium dioxide and zinc oxide have been used in
60 the past decade as antibacterial materials to curb antibacterial resistance [8]. Although the
61 antibacterial action of metal/metal oxide nanomaterials seems relevant in the past, these
62 nanomaterials are not chemically inert [9]. This inadequacy may affect the stability and the
63 antibacterial actions of metal/metal oxide nanomaterial, thus it is not recommended for long-
64 term use especially in the clinical application [10].

65 One of the current applications is the use of GO as an antibacterial material. The
66 antibacterial property of GO is attributed to the direct physical and chemical activity of GO
67 on the bacterial membrane [11]. Loss of microbial membrane integrity and the leakage of
68 intracellular content have been reported to be one of the key mechanisms of bacterial
69 inhibition by GO [12]. Therefore, GO may have the potential to be an effective antibacterial
70 material to reduce the excessive use of antimicrobials [13]. Additionally, the difference in the

71 cell wall components of the Gram-positive and Gram-negative bacteria also contributes to the
72 better antibacterial activity of GO towards *S. aureus* than *E. coli* [14, 15]. Although the
73 antibacterial activity of GO is increasingly reported, the detailed mechanism of action is still
74 lacking and poorly understood [16].

75 In this study, GO was prepared and their antibacterial activity was evaluated against
76 Gram-positive (*Staphylococcus aureus*, *Enterococcus faecalis*) and Gram-negative
77 (*Escherichia coli*, *Pseudomonas aeruginosa*) bacteria. Specifically, cell viability and kinetic
78 studies were carried out while field emission scanning electron microscopy (FESEM)
79 techniques were conducted to observe the difference in the bacterial surface morphology
80 before and after exposure to GO. Transmission electron microscopy (TEM) analysis was
81 carried out for the treated bacterial cells to determine the effects of GO on cell morphology.
82 Finally, ATR-FTIR characterizations of untreated and GO-treated bacteria were conducted to
83 examine their interaction mechanisms.

84 Although there were many studies on the antibacterial activity of GO against Gram-
85 positive and Gram-negative bacteria, however the difference in the mechanism was not dealt
86 with [14, 17-20]. Here, we report the difference in the activity of GO towards Gram-positive
87 and Gram-negative bacteria based on FESEM, TEM and LDH analyses. To the best of our
88 knowledge, this is the first report that provides evidence for the dissimilarity in the
89 mechanistic actions of GO. Additionally, we have described the mechanism of action GO
90 towards bacteria at molecular level through ATR-FTIR characterizations of untreated and
91 GO-treated bacteria.

92

93

94 2. Materials and Methods

95 2.1. Materials

96 Graphite powder, H₂SO₄, H₂PO₄, HCl, H₂O₂ and KMnO₄ were purchased from Sigma-
97 Aldrich, USA. Phosphate buffered saline (PBS) was prepared using PBS tablets from Sigma-
98 Aldrich, USA. Tryptic Soy Agar (TSA) and broth (TSB) were prepared using dehydrated
99 bacterial culture media from BD DifcoTM, USA. Bacterial cultures *S. aureus* ATCC 25923, *E.*
100 *faecalis* ATCC 29212, *E. coli* ATCC 25922 and *P. aeruginosa* ATCC 27853 were from the
101 culture collection of Biomedical Science Laboratory, University of Malaya, Kuala Lumpur,
102 Malaysia.

103

104 2.2. Synthesis and characterization of GO

105 GO sheets were prepared through the modified Hummer's method [21, 22]. Ultraviolet
106 absorption spectra were obtained using Lambda 35 (Perkin-Elmer, USA). An aqueous
107 solution of GO was used as the sample for UV-Vis and distilled water was used as the
108 reference. Wavelengths from 200 to 700 nm were used to characterize the GO. Raman
109 spectra of GO sheets were obtained using a Renishaw inVia Raman microscope (UK) with an
110 excitation laser wavelength of 325 nm. The excitation was conducted with a He-Ne laser in
111 the regions of 1000 to 2200 cm⁻¹. ATR-FTIR characterization of GO was done using
112 Spectrum 400 IR spectrometer equipped with diamond crystal (Perkin Elmer, USA). The
113 ATR-FTIR spectra were recorded with a resolution of ± 4 cm⁻¹ and a scan number of 12 in
114 the range of 4000 to 400 cm⁻¹.

115 2.3. Bacterial culture conditions

116 The bacterial stock cultures were revived and streaked on Tryptic Soy Agar (TSA) plates to
117 check for purity. The culture plates were incubated overnight at 37 °C. A single colony from

118 the overnight TSA was picked and used to inoculate 10 mL Tryptic Soy Broth (TSB). The
119 inoculated broth was incubated overnight at 37 °C with agitation (150 rpm).

120 2.4. *Bacterial Viability Assay*

121 An aliquot of 5 mL of bacterial cultures (10^8 cfu) was incubated with GO of varying
122 concentrations ranging from 5 to 140 $\mu\text{g mL}^{-1}$ for 4 h at 37 °C with agitation (150 rpm). At
123 the end of the designated time period, an aliquot of 100 μL was withdrawn and serially
124 diluted (1:10) in 0.8% saline solution. Serially diluted cell suspensions were plated onto the
125 TSA and incubated overnight at 37 °C to determine the bacterial counts (cfu). The assay was
126 carried out in triplicates of three independent experiments and the results were averaged. The
127 degree of bacterial inactivation was calculated using the formula: $(T_0 - T) / T_0$ where T_0 is the
128 number of bacteria in the GO-free reaction and T is the residual bacteria in the reaction
129 medium at a certain GO concentration. Three independent replicates were conducted for the
130 assay.

131 2.5. *LDH Cytotoxicity Assay*

132 The release of LDH cytotoxicity assay was conducted to determine the degree of membrane
133 damage of bacteria once treated with GO. Membrane integrity of treated bacteria was
134 evaluated using LDH Cytotoxicity Assay Kit (Thermo Fisher Scientific, Massachusetts,
135 USA). Bacterial cultures (10^8 cfu) were incubated with GO suspension of varying
136 concentration ranging from 5 – 140 $\mu\text{g mL}^{-1}$ for 4 h at 37 °C with agitation (150 rpm). At the
137 end of the time period, 50 μL of each reaction mixture were transferred to a 96-well plate and
138 the assay was carried out according to the manufacturer's instructions. The absorbance was
139 measured using a microplate spectrophotometer (Epoch-BioTek, Vermont, USA). Untreated
140 bacterial cultures were regarded as negative control and three independent experiments were
141 performed with replicates and the results were averaged.

142

143

144 2.6. *Time-kill assay*

145 Standardized bacterial cultures (10^8 cfu) were incubated with $10 \mu\text{g mL}^{-1}$ of GO suspension
146 at 37°C with gentle agitation (100 rpm). At the end of selected time periods (2 h, 4 h, 6 h and
147 8 h), $100 \mu\text{L}$ of the bacterial culture was withdrawn and serially diluted (1:10) in 0.8% saline
148 solution. Serially diluted cell suspensions were then plated onto the TSA and incubated
149 overnight at 37°C . Three independent experiments were carried out in triplicates and the
150 results were averaged.

151 2.7. *Observation of bacterial cell morphology upon GO treatment*

152 GO treated and untreated bacterial cells were retrieved from respective experiments for
153 further surface morphology observations. Briefly, $1 \mu\text{L}$ of the bacterial suspension ($\sim 10^8$ cfu
154 mL^{-1}) were treated with 4 % glutaraldehyde (GLA) for 30 minutes, washed with cacodylate
155 buffer and further fixed with 1% Osmium tetroxide for another 30 minutes. The fixed
156 bacterial cells were then gradually dehydrated with ethanol using increasing concentrations
157 ranging from 30%, 50%, 70%, 80%, 90%, and finally 100%. Each ethanol wash was
158 performed for 15 minutes and finally, the completely dried bacterial cells were sputter coated
159 with gold for FESEM observations (FEI, Quanta FEG 650) at a working distance around 9
160 mm, with an acceleration voltage of 20kV. The GO treated bacterial isolates were also
161 observed under TEM (Carl Zeiss, LEO LIBRA 120). For the TEM sample preparation,
162 treated bacterial cells were fixed with 4 % GLA for more than 4 h and washed with
163 cacodylate buffer, fixed with 1% Osmium tetroxide for 2 h and washed again with cacodylate
164 buffer. The bacterial cells were then dehydrated through a graded series of ethanol, treated

165 using propylene oxide and finally embedded in Epon. Thin sections were cut through
166 ultramicrotome, stained with uranyl acetate, air-dried and viewed under TEM.

167

168 2.8. *ATR-FTIR characterizations of GO and bacteria interactions*

169 Bacterial cultures were treated with $10 \mu\text{g mL}^{-1}$ of GO for 4 h as described in the previous
170 section. An aliquot of 100 μL of the GO-treated and untreated bacterial (control) cultures was
171 aseptically dropped onto glass slides, respectively and left to dry. The thin film was analyzed
172 through Spectrum 400 IR spectrometer equipped with diamond crystal (Perkin Elmer, USA).
173 Spectra were recorded with a resolution of $\pm 4 \text{ cm}^{-1}$ and scan number of 12 in the range of
174 4000 to 400 cm^{-1} .

175 3. **Results and Discussion**

176 3.1. *Characterizations of GO*

177 The modified Hummer's method has enabled the formation of an oxidized graphite
178 material that could be further sonicated to form an aqueous suspension of GO. The prepared
179 GO sheets were characterized using ultraviolet adsorption spectroscopy. As seen from
180 Fig.1(a), a peak which corresponds to the $\pi - \pi^*$ plasmon was observed at around 240 nm due
181 to sp^2 clusters of the GO and linking units such as C=C, C=O, and C-O bonds. The shoulder
182 band from 290 nm to 300 nm can be attributed to the $n - \pi^*$ transitions of C = O bonds [23,
183 24], consistent with the findings reported by Gupta *et al.* [25] and Luo *et al.* [26]. Raman
184 spectroscopy is a powerful nondestructive technique and is a very useful optical approach to
185 distinguish the ordered and disordered structure of carbonaceous materials [27, 28]. The
186 Raman spectrum of graphene oxide is shown in Fig. 1(b). Two clear bands at 1416 cm^{-1} and
187 1598 cm^{-1} are the dominant vibrational modes corresponding to the D and G bands of carbon,

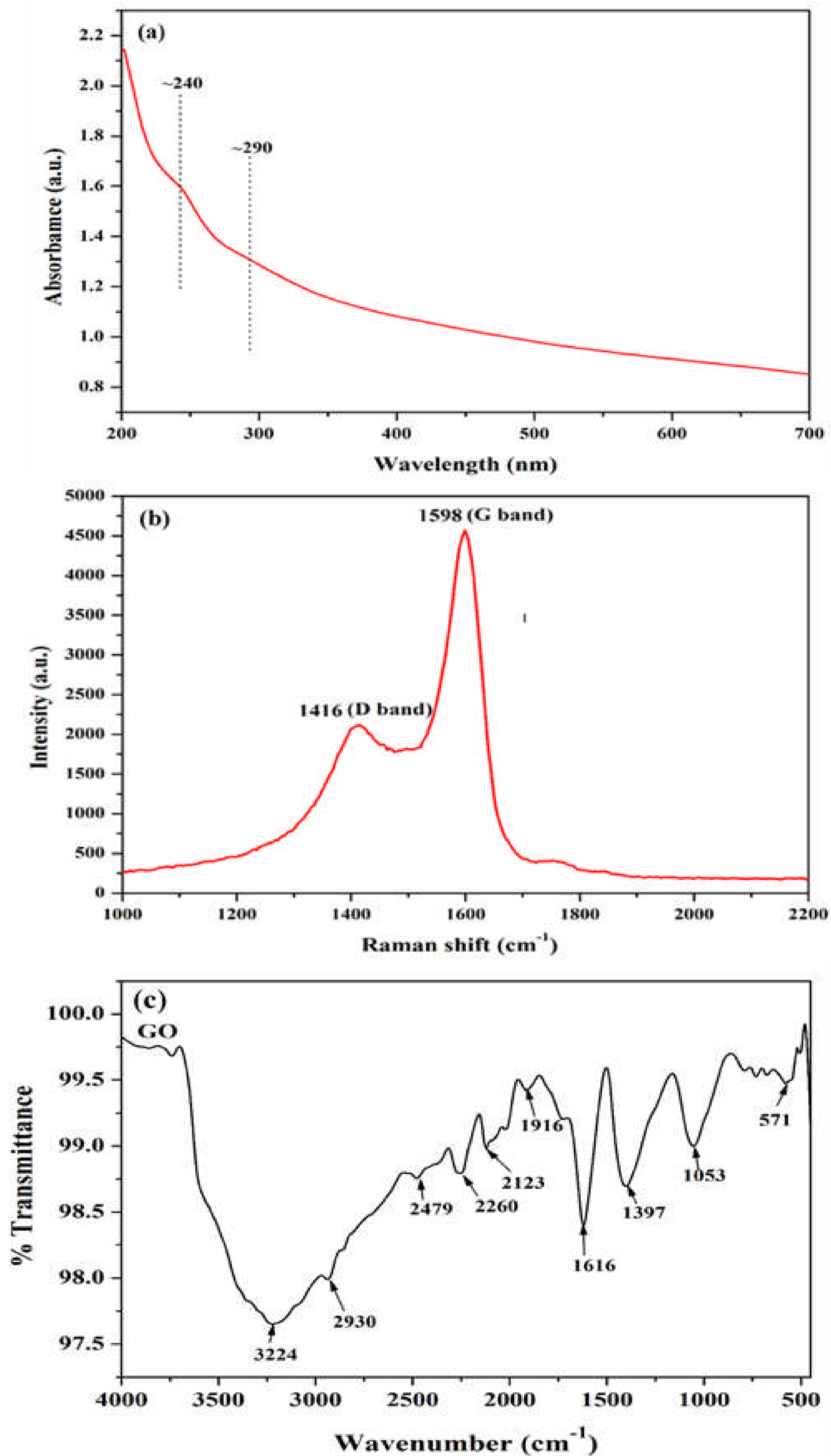
188 respectively [18]. The intense G band at 1598 cm^{-1} is common to all sp^2 carbon forms and is
189 attributed to the optically allowed E_{2g} phonon. The weak D band at 1416 cm^{-1} is ascribed to
190 the mode of the κ -point phonons of A_{1g} symmetry [29], reflecting the degree of defects found
191 on the structure. Raman spectroscopy is mostly used to acquire structural data on carbon
192 materials [30]. The strong band (G) is due to the sp^2 -bonded carbon regions while the weaker
193 band (D) reflects the degree of defects found on the structure [31].

194 The ATR-FTIR spectrum of GO is shown in Fig. 1(c). The presence of the bands in
195 this spectrum is associated with the functional groups of GO. Vibration modes that are based
196 on the configuration of oxygen which include the OH, C-OH, COOH and C-O functional
197 groups are observed in the GO spectrum. The peak observed at 3224 cm^{-1} could be attributed
198 to the presence of carboxyl O-H stretching vibration mode. This peak appeared broad as it
199 overlaps with absorption peaks that correspond to O-H stretching due to the presence of
200 absorbed water molecules and alcohol groups [32]. The asymmetric CH_2 stretching of GO
201 appears at 2930 cm^{-1} and the band that appears as a shoulder peak at 1735 cm^{-1} is attributed to
202 C=O stretch of carboxyl group [33]. The bands at 1397 cm^{-1} and 1053 cm^{-1} corresponds to C-
203 OH and C-O stretching vibrations, respectively [34].

204

205

206



207

208 **Fig. 1.** Characterization of synthesized GO using UV-Vis and Raman spectroscopy. (a) UV-
 209 Vis spectrum of GO; absorbance peak of $\pi - \pi^*$ plasmon is observed at 240 nm. (b) Raman
 210 spectrum of GO; G band arises due to the sp^2 -bonded carbon regions and the D band reflects
 211 the degree of defects found on GO. (c) ATR-FTIR spectrum of GO; Functional groups of
 212 OH, COOH, C-OH and C-O are indicated at 3224 cm^{-1} , 1735 cm^{-1} , 1397 cm^{-1} and 1053 cm^{-1} ,
 213 respectively.

214 3.2. Concentration-dependent activity of GO

215 The antibacterial activity of GO was assessed by exposing selected Gram-positive and
216 Gram-negative bacteria to various concentrations of an aqueous suspension of GO ranging
217 from 0 to 140 $\mu\text{g mL}^{-1}$ for a fixed time-period (4 hours). The line graph in Fig. 2(a) clearly
218 depicts the reduction in the number of cells with an increasing GO concentration for all
219 bacterial strains. The cfu counts indicated that GO has almost completely inhibited the
220 bacterial growth of all strains as seen in the line graph, but the inactivation rate differed
221 among individual bacteria at lower concentrations. Increasing concentrations of GO nearly
222 inactivated 99.9% of all bacteria, whereas *S. aureus* was almost fully inactivated at GO
223 concentrations of 5 $\mu\text{g mL}^{-1}$ compared to other strains. More than 99.9% reduction (> 3 log
224 reductions) in colony counts signifies the bactericidal effect of the GO sheets. Similar
225 observations were made by Akhavan *et al* [14] who reported that *S. aureus* cells have higher
226 susceptibility to GO nanowalls compared to *E. coli*. They reported that the RNA efflux was
227 higher for *S. aureus* than for *E. coli* when exposed to the same concentrations of GO [14].

228 Additionally, membrane integrity of GO treated bacterial cultures was measured by
229 monitoring the release of LDH into the reaction medium after treatment. LDH cytotoxicity
230 assay is commonly used to evaluate the loss of membrane integrity of cells after treatment
231 with toxic compounds [35]. It was found that exposure of bacteria to increasing
232 concentrations of GO enhanced the levels of LDH detected in the medium. This was noted
233 for all bacteria for increasing GO concentrations however differences in the levels of
234 detectable LDH among the bacterial cultures were noted as shown in Fig. 2(b). Higher release
235 of LDH was observed for the Gram-positive isolates (*S. aureus* and *E. faecalis*) compared to
236 the Gram-negative isolates (*E. coli* and *P. aeruginosa*). At 10 $\mu\text{g mL}^{-1}$ of GO, 92% and
237 83.3% of cytotoxicity level were noted for *S. aureus* and *E. faecalis* respectively while

238 cytotoxicity levels of 66.7% and 58.3% were noted for *E. coli* and *P. aeruginosa*
239 respectively.

240 In this study, we have tested two Gram-positive bacteria *S. aureus* and *E. faecalis* and
241 two Gram-negatives *E. coli* and *P. aeruginosa*. Our study indicated that the degree of
242 bacterial inactivation followed the order; *S. aureus* > *E. faecalis* > *E. coli* > *P. aeruginosa* in
243 a descending trend. Evidently, membrane structure plays a definite role in determining the
244 antibacterial activity of GO [14]. Increasing GO concentrations resulted in a reduction in the
245 viability of all strains and enhanced release of LDH, most notably for *S. aureus* and the least
246 towards *P. aeruginosa*, therefore the bactericidal activity of GO is concentration-dependent.
247 This observation concurred with other reports [23, 36, 37]. The higher concentrations of GO
248 provided increased contact with bacterial cells in which the abundant GO sheets could entrap
249 bacterial cells through the wrapping mechanism.

250 The wrapping mechanism explains that GO separates the bacterial cells from the
251 nutrients that are present in the growth medium, thus inhibiting cell proliferation resulting in
252 cell death [31, 38]. As GO concentrations of 10 $\mu\text{g mL}^{-1}$ was able to inactivate more than
253 60% of live cells, this concentration was selected for subsequent experiments. A similar study
254 also reported that 10 $\mu\text{g mL}^{-1}$ of GO suspension was able to exert toxic effects towards
255 bacteria as higher concentrations would possibly cause indirect toxic effects through cell
256 entrapment mechanism which separates bacterial cells from the reaction medium [10].

257

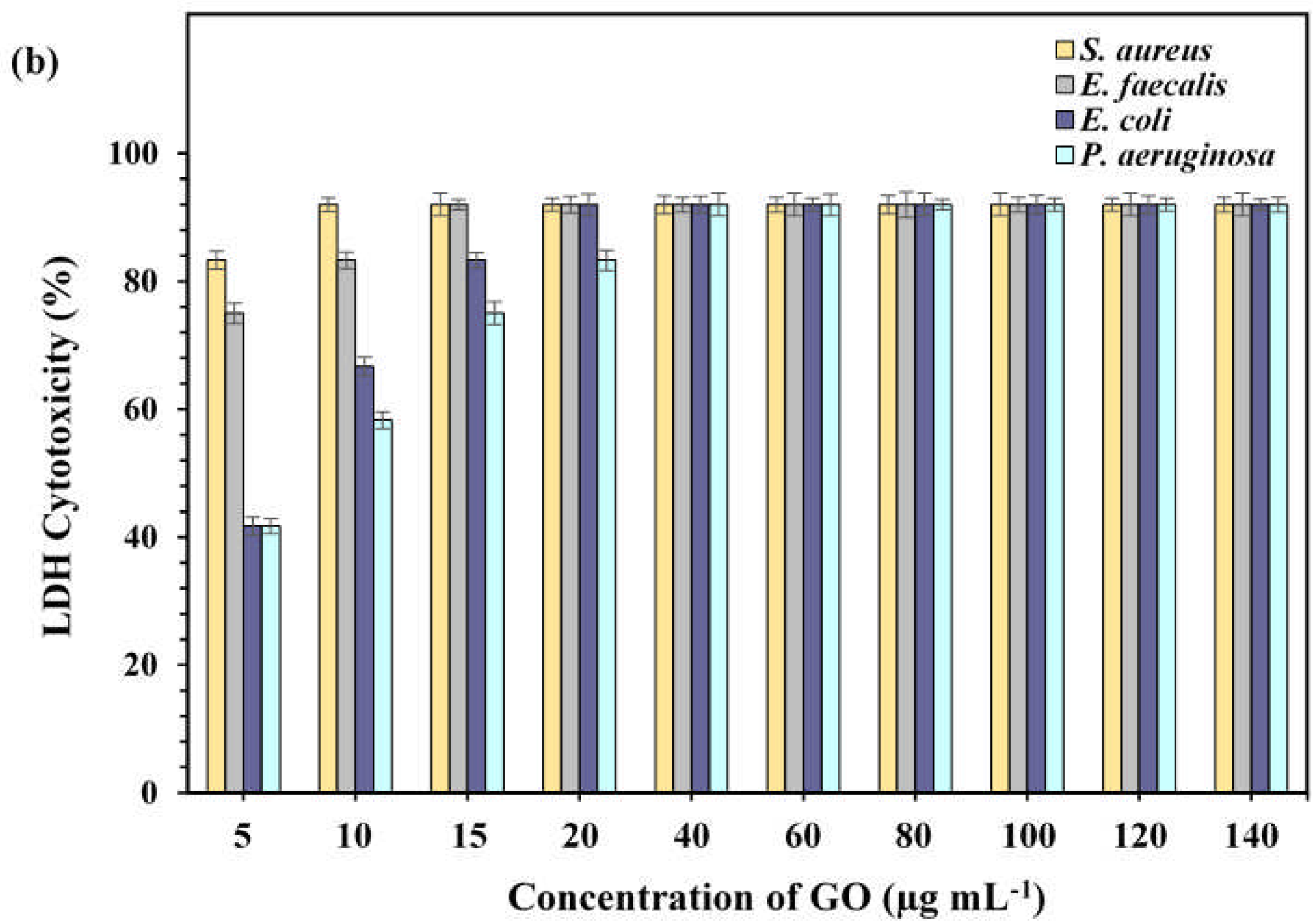
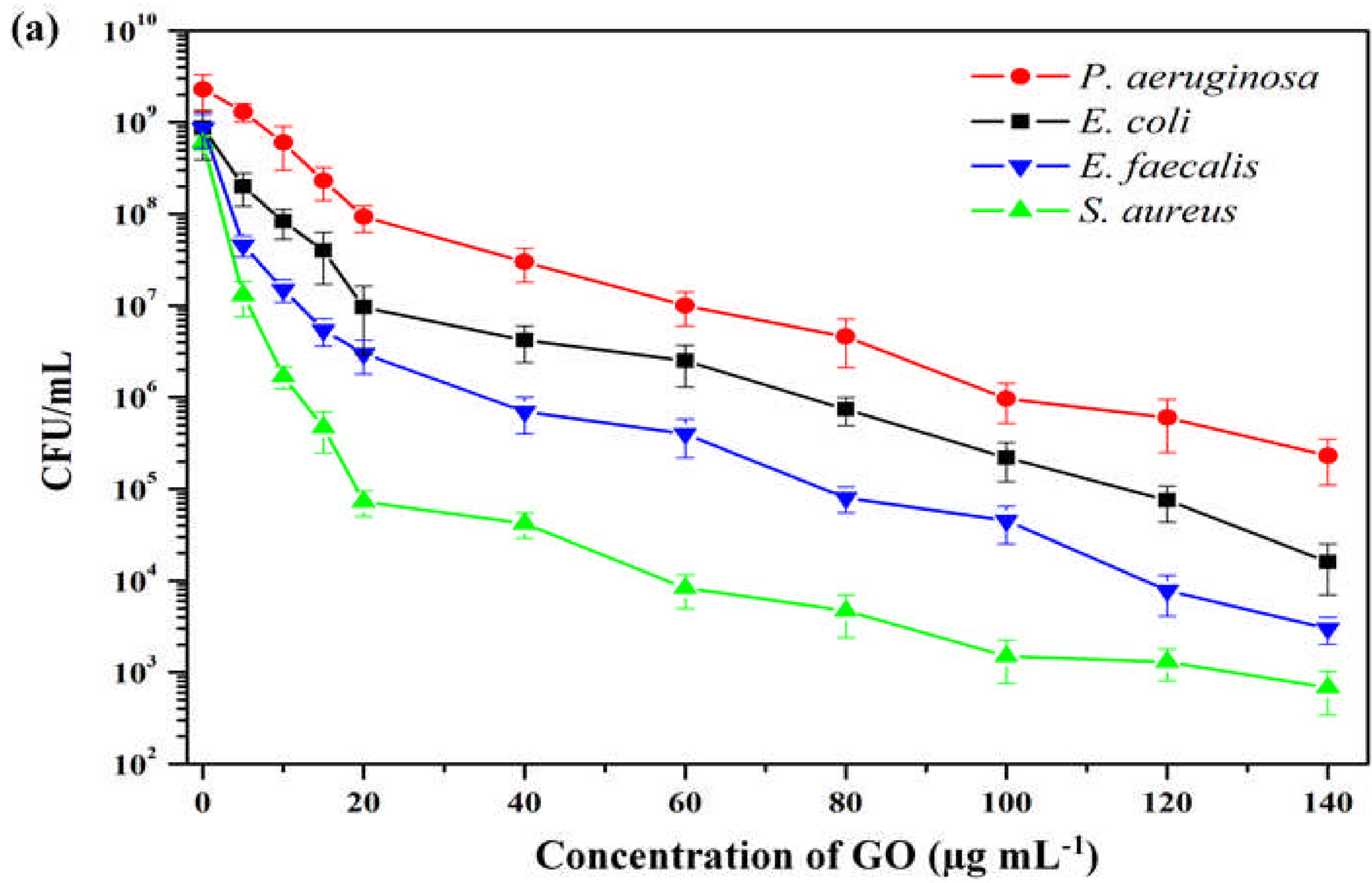
258

259

260

261

262



263

264 **Fig. 2.** Viability curve and LDH cytotoxicity analyses of bacteria after exposure to GO for 4
265 h. (a) A sharp decrease in the viability was observed at GO concentration of $10 \mu\text{g mL}^{-1}$ and
266 deteriorates further as the concentration of GO increases. (b) Increased levels of LDH was
267 measured for increasing concentrations of GO.

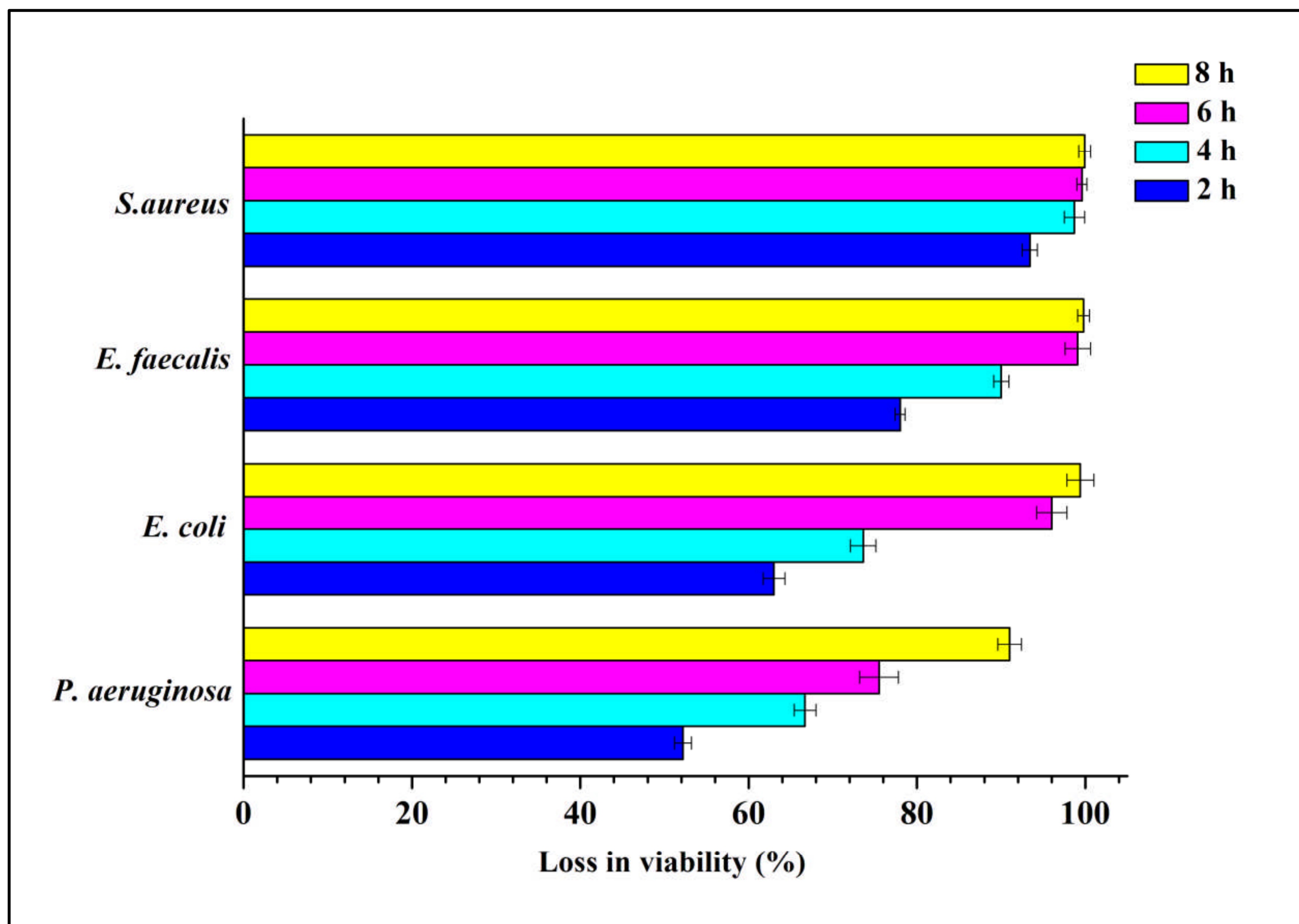
268

269 3.3. Time-dependent activity of GO

270 Time-dependent assays were performed for 8 h with a 2-hour interval time at a fixed
271 GO concentration ($10 \mu\text{g mL}^{-1}$) for all the tested strains. Loss of viability increased with a
272 longer period of incubation as all strains recorded the highest amount of cell death at the 8th
273 hour (Fig. 3). This time-dependent assay also followed the same order of inactivation; *S.*
274 *aureus* > *E. faecalis* > *E. coli* > *P. aeruginosa*. A large portion of cell death occurred at 4 h of
275 incubation and this time-period was used in the subsequent investigations in this work to
276 explore the interactions of GO. Furthermore, Gurunathan *et al.* [23] and Liu *et al.* [37] also
277 described that a major proportion of cell death occurred in the early hours of incubation time
278 which is consistent with our study. This phenomenon suggests that increasing incubation time
279 contributes to longer interaction time and improved contact of GO sheets towards bacterial
280 cells. Although more than 60% viability loss were seen at the 4th hour, better contact mediates
281 enhanced antibacterial activity and this has resulted in major cell loss especially at the 8th
282 hour of incubation. Additionally, with increasing time of contact, the overall proliferation of
283 bacteria may be hindered because a large proportion of bacteria were rendered non-viable at
284 early hours of incubation time. Therefore, our results indicated that the antibacterial activity
285 of GO is concentration- and time-dependent.

286

287



288

289 **Fig. 3.** Time kill assay of bacteria after exposure to GO for several time periods (2 h, 4 h, 6 h
 290 and 8 h). Increase in the incubation time improves bacterial cell contact with GO and this
 291 leads to higher percentage of cell death.

292

293

294

295

296

297

298

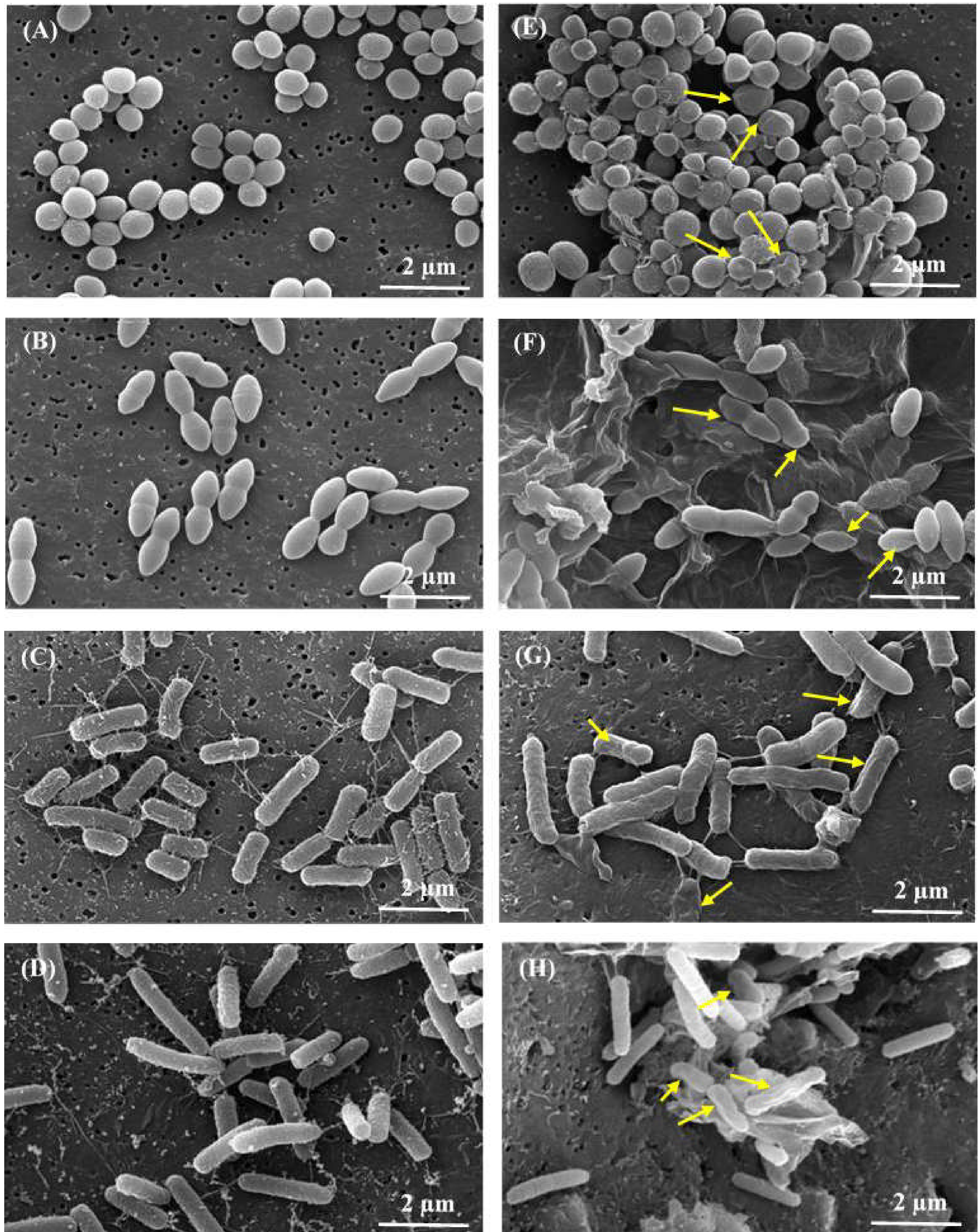
299

300 3.4. Visualization of the bacterial cell upon exposure to GO

301 FESEM characterizations were conducted to investigate the interactions between the
302 bacterial cell membrane and GO sheets. Fig. 4A – 4D represent untreated bacterial cells while
303 Fig. 4E - 4H show the treated cells. FESEM images revealed that untreated bacterial cells
304 were observed to have intact cell membrane compared to bacterial cells that were treated with
305 GO. Treated bacteria cells showed deformed shapes for all strains which indicated
306 compromised membrane integrity and resulted in eventual cell death.

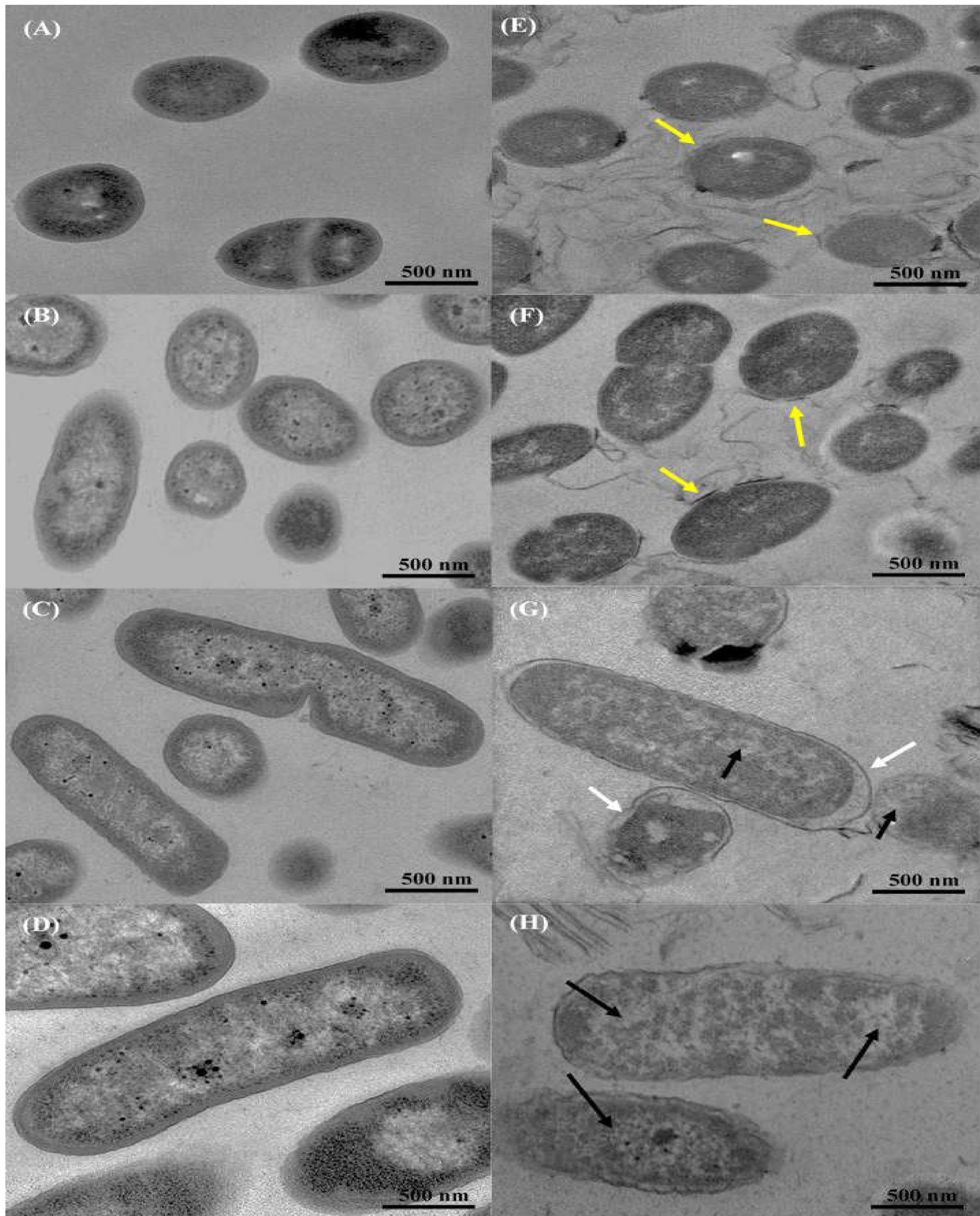
307 Besides, TEM analyses were carried out to monitor morphological changes in the
308 bacterial cells after treatment with GO. Fig. 5A – 5D show the TEM images of untreated
309 bacteria while Fig. 5E – 5H indicate the mechanism of interaction of GO towards bacterial
310 cells. The degree of membrane disruptions and mechanism of action vary according to the
311 type of bacteria. A clear difference in the degree of membrane damage and methods of GO
312 interactions could be observed in the FESEM and TEM images between Gram-positive and
313 Gram-negative bacteria. Large clusters of Gram-positive *S. aureus* and *E. faecalis* appeared
314 to be entrapped by numerous GO sheets in both the FESEM and TEM images. The wrapping
315 mechanism of bacterial cells *via* GO sheets is a documented antibacterial mechanism of
316 action where the cells are actively isolated from the nutrient medium and undergo cell death
317 [31]. In our study, this mechanism was observed clearly for the Gram-positive cells only. As
318 Gram-positive bacteria (*S. aureus* and *E. faecalis*) are usually present in clusters, this
319 increased the surface area of exposure to GO sheets and these cells get trapped leading to the
320 higher death rate. The total surface area of the Gram-positive cells exposed to GO sheets is
321 higher as these bacterial cells (*S. aureus* and *E. faecalis*) usually occur in clusters. Hence
322 more cells are trapped, leading to higher cell death.

323 In contrast, the Gram-negative bacteria suffered hollows and dents on their membrane
324 surface and did not appear to be severely trapped under GO sheets, unlike the Gram-positive
325 cells as observed in Fig. 4G and 4H. Although membrane corrugations have been mainly
326 observed for the Gram-negative bacteria only, loss of viability among *E. coli* and *P.*
327 *aeruginosa* were lower compared to Gram-positive bacteria. In addition, the TEM images of
328 the Gram-negative bacteria in Fig. 5G and 5H were observed to display a decrease in
329 intracellular density which indicated minor loss of cellular components. This type of
330 membrane damage is the effect of physical disruption where destructive extraction of lipid
331 molecules may have occurred. A similar observation was reported by Tu *et al.* [39] that GO
332 treated bacterial cells suffered lower surface phospholipid density due to partial membrane
333 damage. For instance, *E. coli* has been observed to display a slight loss in cytoplasmic
334 content where gaps existed between the cytoplasm and cell wall in the TEM images (Fig.
335 5G). Similar observations were made by Hu *et al.* [40] and Li *et al.* [41] where bacterial cells
336 treated with GO appear to have suffered a loss in cellular integrity along with leakage of
337 cytoplasmic content. Liu *et al.* [37] indicated that the membrane damage happens only after a
338 direct contact with graphene-based materials and the damage appears to be irreversible. The
339 difference in the loss of viability between Gram-positive and Gram-negative bacteria may be
340 explained by the tendency of the Gram-positive bacteria to form cell clusters besides the
341 apparent difference in the cell wall structure. In contrast, Gram-negative bacteria are usually
342 present in single or paired cells, thus a lesser number of bacterial cells will be exposed to GO
343 at any given time, hence lower viability loss for the Gram-negative bacteria was found in this
344 study [42]. Therefore, the antibacterial potential of GO is influenced by the degree of contact
345 between bacterial cells and GO sheets. Similarly, a study conducted by Perreault *et al.* [31]
346 also reported that the close contact between the GO sheets and bacteria cells could
347 compromise the integrity of bacterial membranes.



348

349 **Fig. 4.** FESEM images of bacteria cells before and after exposure to GO. A to D represent
 350 untreated bacteria and E to H represent GO-treated bacterial cells. (A and E; *S. aureus*, B and
 351 *E. faecalis*; C and G; *E. coli*, D and H; *P. aeruginosa*.) Yellow arrows indicate membrane
 352 damage that was observed under FESEM analysis for GO-treated cells only.



353

354 **Fig. 5.** TEM analysis of bacterial cells before and after exposure to GO. A - D represent
 355 untreated bacteria and E to H represent GO-treated bacteria. (A and E; *S. aureus*, B and F; *E.*
 356 *faecalis*; C and G; *E. coli*, D and H; *P. aeruginosa*). Yellow arrows indicate attachment of
 357 GO sheets onto bacterial cells to potentiate antibacterial mechanism. White arrows show
 358 detachment of cell membrane that may have been caused by leakage of cell content. Black
 359 arrows indicate lower density of lipids that may have been caused by partial membrane
 360 damage.

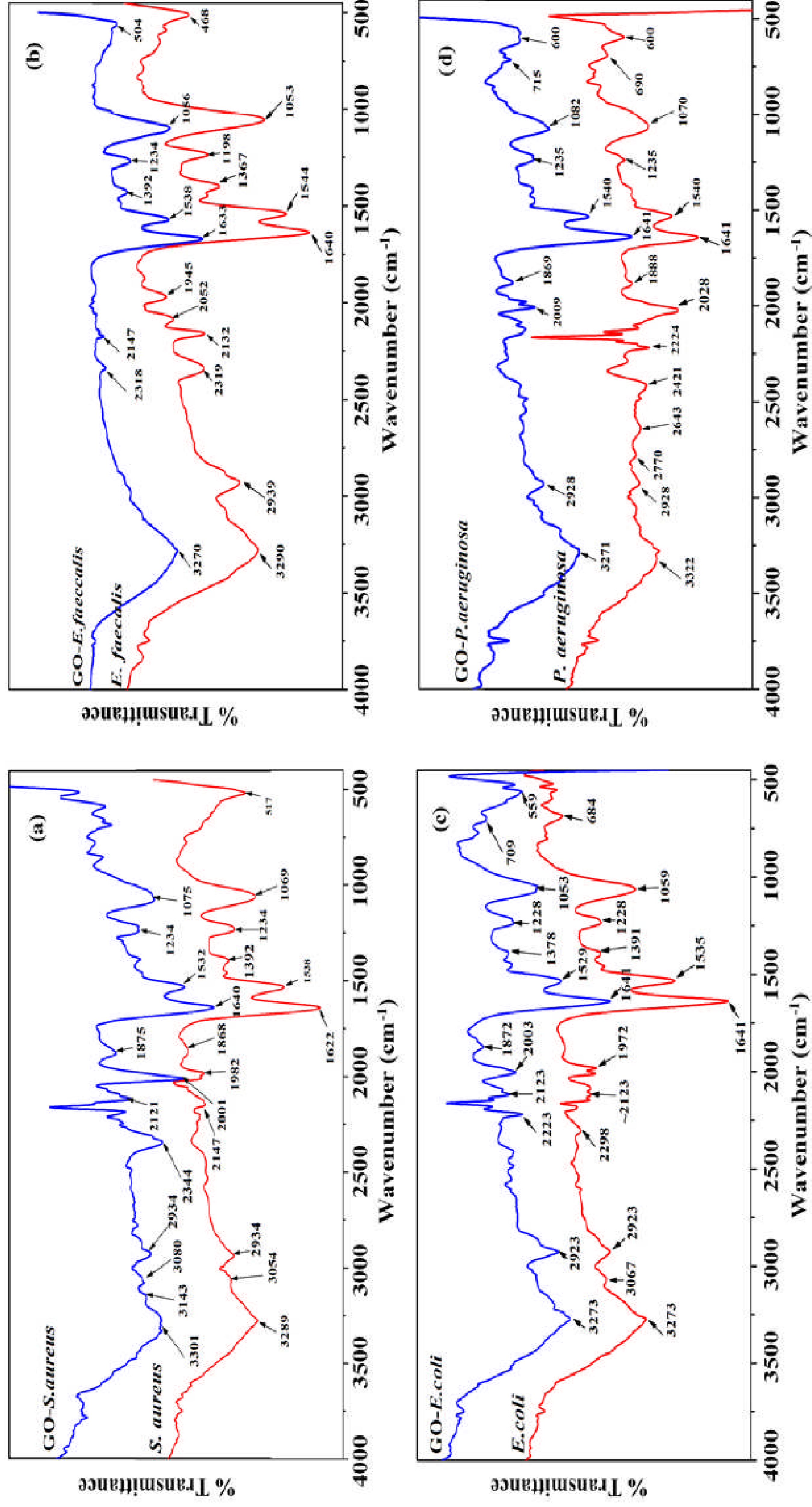
361 3.5. ATR-FTIR characterizations of GO and bacteria interactions

362 ATR-FTIR spectra of bacterial cells are usually conducted to analyze the surface
363 chemistry and functional groups that are present on the cell walls of the bacteria [43]. This
364 technique is commonly used for the identification, detection and classification of bacteria [44,
365 45]. It is also used to detect changes at the molecular level in bacterial cell wall structure. The
366 ATR-FTIR spectra of untreated and GO-treated bacterial cells were analyzed to deduce the
367 different actions of GO on Gram-positive and Gram-negative bacteria.

368 Amongst the bands that exhibited clear differences, the 2344 cm^{-1} band in GO-*S.*
369 *aureus* was assigned to the O-H stretching due to the carboxylic acid which is also present in
370 the GO framework [46]. However, the intensity of the peak was reduced and the peak was
371 observed to be shown at 2260 cm^{-1} in the bare GO spectrum (Fig. 6). The primary and
372 secondary amides (region II) of *S. aureus* occurred at 1622 cm^{-1} and 1538 cm^{-1} , respectively
373 due to the stretching vibrations of C=O and N-H [47]. The intensity of both C=O and N-H
374 bands decreased after the introduction of GO. Additionally, the presence of amino acid
375 functional group at 517 cm^{-1} (region V) which is due to the COO^- and the symmetric C=O
376 stretching of amino acids at 1392 cm^{-1} (region III) were diminished in the GO-*S. aureus*
377 spectrum as shown in Fig. 6(a) [48]. The exposure of GO in the *S. aureus* culture has
378 introduced changes in the carboxylic group of fatty acids, primary and secondary amides of
379 proteins, peptides and amino acids. This might have played a role in causing more damage to
380 the cell wall of these bacteria. The ATR-FTIR spectra of *E. faecalis* and GO-*E. faecalis* are
381 shown in Fig. 6(b). The presence of the characteristic bands of C-H asymmetric of CH_2 in
382 fatty acids at 2939 cm^{-1} in GO-*E. faecalis* spectrum has almost disappeared [46].
383 Furthermore, the O-H stretching vibration due to carboxylic acid at 2319 cm^{-1} and C \equiv C
384 stretching vibration of monoalkyl acetylene at 2132 cm^{-1} have also been reduced in GO-*E.*

385 *faecalis* spectrum [34]. The decrease in the intensity of the peaks from region II to region V
386 reflects the chemical transformation taking place after the treatment of *E. faecalis* with GO.

387 Fig. 6(c) shows the ATR-FTIR spectra of *E. coli* and *E. coli* treated with GO. The
388 peak at 2923 cm^{-1} in *E. coli* spectrum is due to the presence of C-H stretching in aliphatic
389 compounds of cell walls such as lipids mainly along with a minor contribution from proteins,
390 carbohydrates and nucleic acids [34]. This peak, however, has intensified in the GO - *E. coli*
391 and GO -*P. aeruginosa* spectra as well. The intensity of amide II (protein N-H bend, C-N
392 stretch) peak at 1535 cm^{-1} in GO-*E. coli* spectrum has noticeably reduced [49]. Moreover, the
393 peak attributed to COO⁻ symmetric stretch in amino acid side chains and fatty acids at 1391
394 cm^{-1} slightly reduced and have shifted to 1378 cm^{-1} . Furthermore, a P=O asymmetric
395 stretching band which appeared at 1228 cm^{-1} is mainly due to nucleic acids with some
396 influence from phospholipids [50]. These peaks do not fluctuate before and after the
397 treatment. The strong absorption band that appeared at 1059 cm^{-1} may be associated with
398 PO²⁻ symmetric stretching from nucleic acids and phospholipids and this band decreases in
399 intensity after GO treatment [51]. Similarly, the PO²⁻ symmetric stretching band appeared at
400 1070 cm^{-1} for *P. aeruginosa* and this band decreased in intensity after GO exposure. The
401 ATR-FTIR spectra of *P. aeruginosa* and GO-*P. aeruginosa* is shown in Fig. 6(d). In contrast
402 to other bacteria, the amide I and amide II bands of *P. aeruginosa* after the GO treatment
403 have intensified. Therefore, the results clearly demonstrated the differential effects of GO on
404 the functional groups on the surface of the bacterial cell walls.



405 **Fig. 6.** ATR-FTIR characterizations of untreated and GO treated bacterial cultures. The spectra show the differences in the intensity of
 406 functional groups that are present on the surface of bacterial cell wall before and after treatment with GO. (a) ATR-FTIR spectra of untreated
 407 and treated *S. aureus*; (b) ATR-FTIR spectrum of untreated and treated *E. faecalis*; (c) ATR-FTIR spectrum of untreated and treated *E. coli*; (d)
 408 ATR-FTIR spectrum of untreated and treated *P. aeruginosa*.

409 3.6. Mechanism of action of GO towards bacteria

410 Our study showed that the antibacterial effects of GO on Gram-positive bacteria were
411 greater compared to Gram-negative bacteria. Additionally, ATR-FTIR characterizations of
412 untreated and treated bacterial isolates confirmed molecular interactions that occurred
413 between the bacterial cell and GO sheets. Briefly, the exposed part of the bacteria that is
414 available for the GO to immediately act on is the outer membrane layer for Gram-negative
415 bacteria and the peptidoglycan layer for Gram-positive bacteria [52]. This dissimilarity plays
416 a role in determining the type of interactions that occur between the two classes of bacteria
417 with GO. Similar observations were made by Deokar *et al.* [15] who reported that Gram-
418 positive *S. aureus* was more susceptible towards the antibacterial activity of carbon nanotube
419 compared to Gram-negative *E. coli*. The authors suggested that Gram-positive bacteria
420 interacted with these nanomaterials through electrostatic or hydrogen bonding besides
421 physical piercing of cell membrane while Gram-negative bacteria interacted with the
422 nanomaterial through direct physical contact only [15].

423 The thick peptidoglycan layer in Gram-positive bacteria and additional presence of
424 teichoic acids, lipoids and amino acids on the surface of these bacteria may have contributed
425 to the added interaction between the Gram-positive bacteria and GO [15, 53]. The
426 peptidoglycan layers have an adherence characteristic which may have caused this layer to
427 behave as a chelating agent [54] and this can be attributed to the presence of surface proteins
428 such as teichoic acids and adhesins [55]. In general, Gram-positive bacteria such as *S. aureus*
429 and *E. faecalis* are commensal bacteria on humans where the former resides on the skin and
430 the latter resides in the gastrointestinal tract [56, 57]. However, these bacteria are also
431 opportunistic pathogens which could cause invasive infections when there is a breach in the
432 epithelial lining by adhering to the host tissues to initiate bacterial colonization [55].
433 Therefore, we propose that similar adhering mechanism has prompted interactions with the

434 GO sheets, whereby the surface proteins on the peptidoglycan layer have interacted with GO.
435 The interactions of GO with Gram-positive bacteria may have contributed to the mechanical
436 wrapping of GO sheets onto *S. aureus* and *E. faecalis* as indicated in Fig. 7(A) and 7(B).
437 Thus, the peptidoglycan layer tends to interact with GO sheets once it is in close proximity
438 and this necessitates adherence of GO onto the bacterial membrane.

439 FESEM images in Fig. 4 show that GO sheets are observed to entrap *S. aureus* and *E.*
440 *faecalis*, however, this is not the case for Gram-negative *E. coli* and *P. aeruginosa*. The outer
441 membrane layer on Gram-negative bacteria forms an extra protective layer for these bacteria
442 from interacting closely to GO sheets. Although membrane damage to *E. coli* and *P.*
443 *aeruginosa* have been observed, mechanical wrapping of these cells was not observed in the
444 FESEM or the TEM images. Therefore, variation in the degree of damage on the bacterial
445 membrane among the Gram-positive and Gram-negative bacteria may be contributory to the
446 type of interaction that occurred during contact between bacteria and GO sheets [15]. The
447 outer membrane is essential to the survival of Gram-negative bacteria as this layer offers
448 protection to the bacteria in a hostile environment including in the presence of antibiotics and
449 it is one of the key reasons that Gram-negative bacteria are generally resistant towards
450 antibiotics [58]. The lipopolysaccharide (LPS) that is found on the outer leaflet of the outer
451 membrane plays a role in the effective exclusion of hydrophobic molecules [55, 59]. It was
452 suggested LPS molecules may contribute to the overall repulsive forces on Gram-negative
453 bacteria through steric repulsion [60].

454 It has been noted that interaction between the bacteria and GO are mainly repulsive as
455 reported by Castrillón *et al.* [61] who investigated the effects of GO - functionalized atomic
456 force microscopy (AFM) probe puncture on *E. coli* cell wall. The repulsive force may have
457 arisen from the electrostatic repulsion from the negatively charged bacterial outer membrane
458 and deprotonated carboxylic acid groups existing on GO [62, 63]. However, sporadic

459 adhesions were measured upon AFM probe pull-off and it was suggested to be due to LPS
460 stretching effects which bridges cell surface and AFM tip upon pull-off [61]. In our study,
461 similar events may have occurred where LPS on the cell surface of Gram-negative bacteria
462 were stretched upon the ensuing repulsive force during interactions between bacteria and GO
463 in the reaction medium. The bridging effects of LPS may have been responsible for the
464 indentations that are observed on the surface of Gram-negative bacteria in the FESEM
465 images in Fig. 4. Correspondingly, an investigation that was conducted to study the
466 puncturing effects of AFM tip on the Gram-negative *Salmonella* Typhimurium managed to
467 survive after multiple puncturing of their cell wall. Lipid bilayers and peptidoglycan layer of
468 the bacteria are suggested to be self-repairing as it retains the integrity, viability and
469 reproductive ability even after repeated puncturing of cell membrane [64].

470

471

472

473

474

475

476

477

478

479

480

481

482
483
484
485
486
487
488
489
490
491
492
493
494
495
496
497
498
499
500
501
502
503
504
505
506
507
508

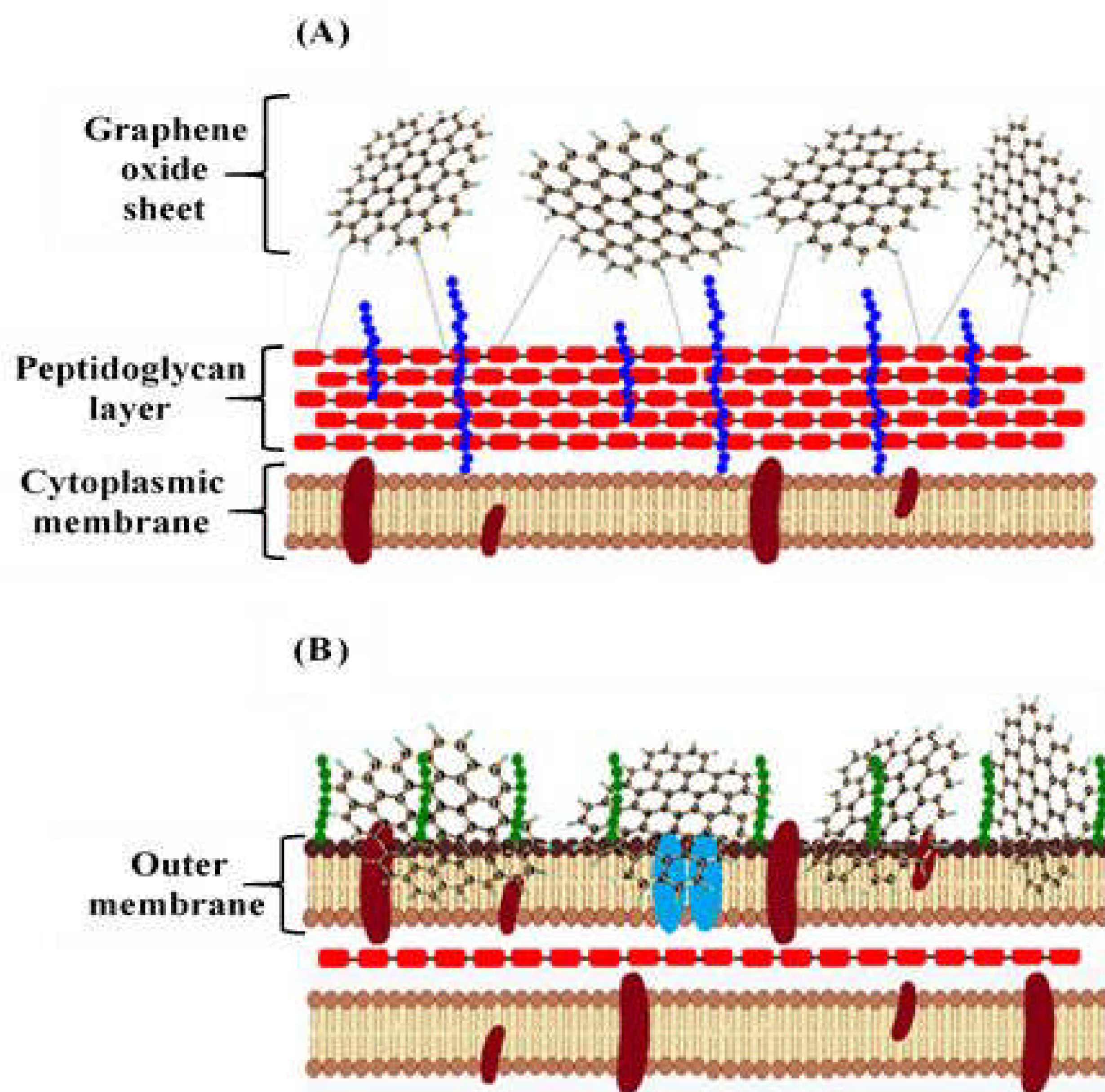


Fig. 7. Schematic diagram of the possible mechanism of action of GO towards Gram-positive and Gram-negative bacteria. (A) mechanical wrapping in Gram-positive bacteria and (B) membrane damage in Gram-negative bacteria.

509 4. Conclusion

510 The antibacterial activity of GO towards *S. aureus*, *E. faecalis*, *E. coli* and *P.*
511 *aeruginosa* indicated that antibacterial activity of GO was concentration and time-dependent.
512 Surface morphology of bacterial cells after exposure of GO showed evidence of membrane
513 disruptions and bacterial entrapment under GO sheets that have contributed to cell death.
514 Additional characterization with ATR-FTIR analysis proved that the interaction of GO with
515 bacterial membrane occurs upon contact, resulting in changes in the IR spectra of untreated
516 and treated bacterial culture. The antibacterial mechanism of GO towards bacteria differed
517 between Gram-positive and Gram-negative bacteria, where the majority of bacterial
518 inactivation of Gram-positive bacteria occurs through bacterial wrapping mechanism. On the
519 other hand, inactivation of Gram-negative bacteria mainly occurs through physical contact
520 which leads to membrane damage. The outer membrane layer in Gram-negative bacteria
521 acted as a protective barrier against GO compared to Gram-positive bacteria. As the
522 antibacterial effects of GO have enormous potential for antimicrobial applications, the
523 mechanism of action of GO towards bacteria must be clearly elucidated to ensure complete
524 bacterial inactivation.

525

526

527

528

529

530

531

532 **Acknowledgements**

533 This work was supported by BKP (BK095-2016) and UMRG (RP045-17AET) grants from
534 University of Malaya and by Fundamental Research Grant Scheme (FP054-2016) from
535 Ministry of Higher Education, Malaysia.

536

537 **Compliance with Ethical Standards:**

538 Funding: This study was funded by University of Malaya through BKP (BK095-2016) and
539 UMRG (RP045-17AET) grants and by the Fundamental Research Grant Scheme (FP054-
540 2016) from Ministry of Higher Education, Malaysia.

541 Conflict of Interest: Thiruchelvi Pulingam, Kwai Lin Thong, Md. Equb Ali, Jimmy Nelson
542 Appaturi, Ignatius Julian Dinshaw, Zhan Yuin Ong and Bey Fen Leo declare that they have
543 no conflict of interest.

544 Ethical approval: This article does not contain any studies with human participants or animals
545 performed by any of the authors.

546 Informed consent: Informed consent was not obtained as no human participants were
547 involved in this study.

548

549

550

551

553 **References**

- 554 1. Wu, X., et al., *Graphene oxide as an efficient antimicrobial nanomaterial for*
555 *eradicating multi-drug resistant bacteria in vitro and in vivo*. Colloids and Surfaces
556 B: Biointerfaces, 2017. **157**: p. 1-9.
- 557 2. Papi, M., et al., *Biomimetic antimicrobial cloak by graphene-oxide agar hydrogel*.
558 Scientific reports, 2016. **6**(1): p. 12.
- 559 3. Zhou, S. and A. Bongiorno, *Origin of the chemical and kinetic stability of graphene*
560 *oxide*. Scientific reports, 2013. **3**: p. 2484.
- 561 4. Liu, S., et al., *Stable aqueous dispersion of graphene nanosheets: noncovalent*
562 *functionalization by a polymeric reducing agent and their subsequent decoration with*
563 *Ag nanoparticles for enzymeless hydrogen peroxide detection*. Macromolecules, 2010.
564 **43**(23): p. 10078-10083.
- 565 5. Liu, Z., et al., *PEGylated nanographene oxide for delivery of water-insoluble cancer*
566 *drugs*. Journal of the American Chemical Society, 2008. **130**(33): p. 10876-10877.
- 567 6. Sun, X., et al., *Nano-graphene oxide for cellular imaging and drug delivery*. Nano
568 research, 2008. **1**(3): p. 203-212.
- 569 7. Yang, K., et al., *Nano-graphene in biomedicine: theranostic applications*. Chemical
570 Society Reviews, 2013. **42**(2): p. 530-547.
- 571 8. Allahverdiyev, A.M., et al., *Coping with antibiotic resistance: combining*
572 *nanoparticles with antibiotics and other antimicrobial agents*. Expert review of anti-
573 infective therapy, 2011. **9**(11): p. 1035-1052.
- 574 9. Vimbela, G.V., et al., *Antibacterial properties and toxicity from metallic*
575 *nanomaterials*. International Journal of Nanomedicine, 2017. **12**: p. 3941.
- 576 10. Gao, Y., et al., *Impact of graphene oxide on the antibacterial activity of antibiotics*
577 *against bacteria*. Environmental Science: Nano, 2017. **4**(5): p. 1016-1024.
- 578 11. Wang, Z., et al., *Carbon nanomaterials-based electrochemical aptasensors*.
579 Biosensors and Bioelectronics, 2016. **79**: p. 136-149.
- 580 12. Pelin, M., et al., *Graphene and graphene oxide induce ROS production in human*
581 *HaCaT skin keratinocytes: The role of xanthine oxidase and NADH dehydrogenase*.
582 Nanoscale, 2018. **10**(25): p. 11820-11830.
- 583 13. Jalali, M., J. Zaborowska, and M. Jalali, *The Polymerase Chain Reaction: PCR,*
584 *qPCR, and RT-PCR*, in *Basic Science Methods for Clinical Researchers*. 2017,
585 Elsevier. p. 1-18.
- 586 14. Akhavan, O. and E. Ghaderi, *Toxicity of graphene and graphene oxide nanowalls*
587 *against bacteria*. ACS Nano, 2010. **4**(10): p. 5731-6.
- 588 15. Deokar, A.R., et al., *Single-walled carbon nanotube coated antibacterial paper:*
589 *preparation and mechanistic study*. Journal of Materials Chemistry B, 2013. **1**(20): p.
590 2639-2646.
- 591 16. Wang, L., C. Hu, and L. Shao, *The antimicrobial activity of nanoparticles: present*
592 *situation and prospects for the future*. International journal of nanomedicine, 2017.
593 **12**: p. 1227.
- 594 17. Hui, L., et al., *Availability of the basal planes of graphene oxide determines whether*
595 *it is antibacterial*. ACS Appl Mater Interfaces, 2014. **6**(15): p. 13183-90.
- 596 18. Nanda, S.S., D.K. Yi, and K. Kim, *Study of antibacterial mechanism of graphene*
597 *oxide using Raman spectroscopy*. Sci Rep, 2016. **6**: p. 28443.

- 598 19. Zou, F., et al., *Wrinkled Surface-Mediated Antibacterial Activity of Graphene Oxide*
599 *Nanosheets*. ACS Appl Mater Interfaces, 2017.
- 600 20. Hou, W.-C., et al., *Antibacterial Property of Graphene Oxide: the Role of*
601 *Phototransformation*. Environmental Science: Nano, 2017.
- 602 21. Huang, N., et al., *Simple room-temperature preparation of high-yield large-area*
603 *graphene oxide*. International journal of nanomedicine, 2011. **6**: p. 3443.
- 604 22. Hummers Jr, W.S. and R.E. Offeman, *Preparation of graphitic oxide*. Journal of the
605 American Chemical Society, 1958. **80**(6): p. 1339-1339.
- 606 23. Gurunathan, S., et al., *Antibacterial activity of dithiothreitol reduced graphene oxide*.
607 Journal of Industrial and Engineering Chemistry, 2013. **19**(4): p. 1280-1288.
- 608 24. Guo, Z., et al., *Toxicity and transformation of graphene oxide and reduced graphene*
609 *oxide in bacteria biofilm*. Science of The Total Environment, 2017. **580**: p. 1300-
610 1308.
- 611 25. Gupta, V., et al., *Higher oxidation level in graphene oxide*. Optik - International
612 Journal for Light and Electron Optics, 2017. **143**(Supplement C): p. 115-124.
- 613 26. Luo, Z., et al., *High Yield Preparation of Macroscopic Graphene Oxide Membranes*.
614 Journal of the American Chemical Society, 2009. **131**(3): p. 898-899.
- 615 27. Shi, P., et al., *Supported cobalt oxide on graphene oxide: Highly efficient catalysts for*
616 *the removal of Orange II from water*. Journal of Hazardous Materials, 2012. **229-**
617 **230**(Supplement C): p. 331-339.
- 618 28. Zhang, M., et al., *Preparation of cobalt silicide on graphene as Pt electrocatalyst*
619 *supports for highly efficient and stable methanol oxidation in acidic media*.
620 Electrochimica Acta, 2015. **161**(Supplement C): p. 48-54.
- 621 29. Zhou, K., et al., *The influence of cobalt oxide-graphene hybrids on thermal*
622 *degradation, fire hazards and mechanical properties of thermoplastic polyurethane*
623 *composites*. Composites Part A: Applied Science and Manufacturing, 2016.
624 **88**(Supplement C): p. 10-18.
- 625 30. Chaiyakun, S., et al., *Preparation and characterization of graphene oxide nanosheets*.
626 Procedia Engineering, 2012. **32**: p. 759-764.
- 627 31. Perreault, F., et al., *Antimicrobial Properties of Graphene Oxide Nanosheets: Why*
628 *Size Matters*. ACS Nano, 2015. **9**(7): p. 7226-36.
- 629 32. Nyquist, R.A. and R.O. Kagel, *Handbook of infrared and raman spectra of inorganic*
630 *compounds and organic salts: infrared spectra of inorganic compounds*. Vol. 4. 2012:
631 Academic press.
- 632 33. Valentini, L., et al., *Deposition of amino-functionalized polyhedral oligomeric*
633 *silsesquioxanes on graphene oxide sheets immobilized onto an amino-silane modified*
634 *silicon surface*. Journal of Materials Chemistry, 2012. **22**(13): p. 6213-6217.
- 635 34. Thirunavukkarasu, R., et al., *Isolation of bioactive compound from marine seaweeds*
636 *against fish pathogenic bacteria Vibrio alginolyticus (VA09) and characterisation by*
637 *FTIR*. Journal of Coastal Life Medicine, 2013. **1**(1): p. 26-33.
- 638 35. Venkatasubbu, G.D., et al., *Toxicity mechanism of titanium dioxide and zinc oxide*
639 *nanoparticles against food pathogens*. Colloids and Surfaces B: Biointerfaces, 2016.
640 **148**: p. 600-606.
- 641 36. Krishnamoorthy, K., et al., *Antibacterial efficiency of graphene nanosheets against*
642 *pathogenic bacteria via lipid peroxidation*. The Journal of Physical Chemistry C,
643 2012. **116**(32): p. 17280-17287.
- 644 37. Liu, S., et al., *Antibacterial activity of graphite, graphite oxide, graphene oxide, and*
645 *reduced graphene oxide: membrane and oxidative stress*. ACS Nano, 2011. **5**(9): p.
646 6971-80.

- 647 38. Zhao, J., et al., *Graphene in the aquatic environment: adsorption, dispersion, toxicity*
648 *and transformation*. Environmental science & technology, 2014. **48**(17): p. 9995-
649 10009.
- 650 39. Tu, Y., et al., *Destructive extraction of phospholipids from Escherichia coli*
651 *membranes by graphene nanosheets*. Nat Nanotechnol, 2013. **8**(8): p. 594-601.
- 652 40. Hu, W., et al., *Graphene-based antibacterial paper*. ACS nano, 2010. **4**(7): p. 4317-
653 4323.
- 654 41. Li, R., et al., *Identification and Optimization of Carbon Radicals on Hydrated*
655 *Graphene Oxide for Ubiquitous Antibacterial Coatings*. ACS Nano, 2016. **10**(12): p.
656 10966-10980.
- 657 42. Barenfanger, J. and C.A. Drake, *Interpretation of Gram stains for the*
658 *nonmicrobiologist*. Laboratory medicine, 2001. **32**(7): p. 368-375.
- 659 43. Davis, R. and L. Mauer, *Fourier transform infrared (FT-IR) spectroscopy: a rapid*
660 *tool for detection and analysis of foodborne pathogenic bacteria*. Current research,
661 technology and education topics in applied microbiology and microbial
662 biotechnology, 2010. **2**: p. 1582-1594.
- 663 44. Rebuffo, C.A., et al., *Reliable and rapid identification of Listeria monocytogenes and*
664 *Listeria species by artificial neural network-based Fourier transform infrared*
665 *spectroscopy*. Applied and environmental microbiology, 2006. **72**(2): p. 994-1000.
- 666 45. Kuhm, A.E., et al., *Application of Fourier transform infrared spectroscopy (FT-IR)*
667 *for the identification of Yersinia enterocolitica on species and subspecies level*.
668 Applied and Environmental Microbiology, 2009.
- 669 46. Kannan, S., *FT-IR and EDS analysis of the seaweeds Sargassum wightii (brown*
670 *algae) and Gracilaria corticata (red algae)*. International Journal of Current
671 Microbiology and Applied Sciences, 2014. **3**(4): p. 341-351.
- 672 47. Bhat, R., *Potential use of fourier transform infrared spectroscopy for identification of*
673 *molds capable of producing mycotoxins*. International journal of food properties,
674 2013. **16**(8): p. 1819-1829.
- 675 48. Garip, S., F. Bozoglu, and F. Severcan, *Differentiation of mesophilic and thermophilic*
676 *bacteria with Fourier transform infrared spectroscopy*. Applied spectroscopy, 2007.
677 **61**(2): p. 186-192.
- 678 49. Suzuki, H., et al., *Functional roles of D2-Lys317 and the interacting chloride ion in*
679 *the water oxidation reaction of photosystem II as revealed by Fourier transform*
680 *infrared analysis*. Biochemistry, 2013. **52**(28): p. 4748-4757.
- 681 50. Lebedeva, O., et al., *Hybrid ion-exchange membranes based on heteroaromatic*
682 *sulfonic acid derivatives*. Petroleum chemistry, 2015. **55**(5): p. 333-338.
- 683 51. Wong, P., et al., *Infrared spectroscopy of exfoliated human cervical cells: evidence of*
684 *extensive structural changes during carcinogenesis*. Proceedings of the National
685 Academy of Sciences, 1991. **88**(24): p. 10988-10992.
- 686 52. Brown, L., et al., *Through the wall: extracellular vesicles in Gram-positive bacteria,*
687 *mycobacteria and fungi*. Nature Reviews Microbiology, 2015. **13**(10): p. 620.
- 688 53. Liang, H., et al., *Metabolic labelling of the carbohydrate core in bacterial*
689 *peptidoglycan and its applications*. Nature communications, 2017. **8**: p. 15015.
- 690 54. Kell, A.J., et al., *Vancomycin-modified nanoparticles for efficient targeting and*
691 *preconcentration of Gram-positive and Gram-negative bacteria*. Acs Nano, 2008.
692 **2**(9): p. 1777-1788.
- 693 55. Silhavy, T.J., D. Kahne, and S. Walker, *The bacterial cell envelope*. Cold Spring
694 Harbor perspectives in biology, 2010. **2**(5): p. a000414.
- 695 56. Kommineni, S., et al., *Bacteriocin production augments niche competition by*
696 *enterococci in the mammalian gastrointestinal tract*. Nature, 2015. **526**(7575): p. 719.

- 697 57. Chiller, K., B.A. Selkin, and G.J. Murakawa. *Skin microflora and bacterial infections*
698 *of the skin*. in *Journal of Investigative Dermatology Symposium Proceedings*. 2001.
699 Elsevier.
- 700 58. Delcour, A.H., *Outer membrane permeability and antibiotic resistance*. *Biochimica et*
701 *Biophysica Acta (BBA)-Proteins and Proteomics*, 2009. **1794**(5): p. 808-816.
- 702 59. Kamio, Y. and H. Nikaido, *Outer membrane of Salmonella typhimurium: accessibility*
703 *of phospholipid head groups to phospholipase c and cyanogen bromide activated*
704 *dextran in the external medium*. *Biochemistry*, 1976. **15**(12): p. 2561-2570.
- 705 60. Nikaido, H., *Molecular basis of bacterial outer membrane permeability revisited*.
706 *Microbiology and molecular biology reviews*, 2003. **67**(4): p. 593-656.
- 707 61. Romero-Vargas Castrillón, S., et al., *Interaction of graphene oxide with bacterial cell*
708 *membranes: insights from force spectroscopy*. *Environmental Science & Technology*
709 *Letters*, 2015. **2**(4): p. 112-117.
- 710 62. Dreyer, D.R., A.D. Todd, and C.W. Bielawski, *Harnessing the chemistry of graphene*
711 *oxide*. *Chemical Society Reviews*, 2014. **43**(15): p. 5288-5301.
- 712 63. Camesano, T.A. and B.E. Logan, *Probing bacterial electrosteric interactions using*
713 *atomic force microscopy*. *Environmental Science & Technology*, 2000. **34**(16): p.
714 3354-3362.
- 715 64. Suo, Z., et al., *Bacteria survive multiple puncturings of their cell walls*. *Langmuir*,
716 2009. **25**(8): p. 4588-4594.

717